ACS APPLIED MATERIALS & INTERFACES

Research Article

www.acsami.org

Red Fluorescent Zinc Oxide Nanoparticle: A Novel Platform for Cancer Targeting

Hao Hong,[†] Fei Wang,[‡] Yin Zhang,[§] Stephen A. Graves,[§] Savo Bou Zein Eddine,[†,∥] Yunan Yang,[†] Charles P. Theuer,[⊥] Robert J. Nickles,[§] Xudong Wang,*[,‡] and Weibo Cai*[,†,§,#]

[†]Department of Radiology, University of Wisconsin-Madison, Madison, Wisconsin 53705-2275, United States

[‡]Department of Materials Science and Engineering, University of Wisconsin-Madison, Madison, Wisconsin 53705-2275, United States

[§]Department of Medical Physics, University of Wisconsin-Madison, Madison, Wisconsin 53705-2275, United States

[∥]Faculty of Medicine and Medical Center, American University of Beirut, Beirut 11072020, Lebanon

[⊥]TRACON Pharmaceuticals, San Diego, California 92122, United States

[#]University of Wisconsin Carbone Cancer Center, Madison, Wisconsin 53705-2275, United States

ABSTRACT: Multifunctional zinc oxide (ZnO) nanoparticles (NPs) with well-integrated multimodality imaging capacities have generated increasing research interest in the past decade. However, limited progress has been made in developing ZnO NP-based multimodality tumor-imaging agents. Here we developed novel red fluorescent ZnO NPs and described the successful conjugation of ^{64}Cu ($t_{1/2}$ = 12.7 h) and TRC105, a chimeric monoclonal antibody against CD105, to these ZnO NPs via well-developed surface engineering procedures. The produced dual-modality ZnO NPs were readily applicable for positron emission tomography (PET) imaging and fluorescence imaging of the tumor vasculature. Their pharmacokinetics and tumor-targeting efficacy/specificity in mice bearing murine breast 4T1 tumor were thoroughly investigated. ZnO NPs with dual-modality imaging properties can serve as an attractive candidate for future cancer theranostics.

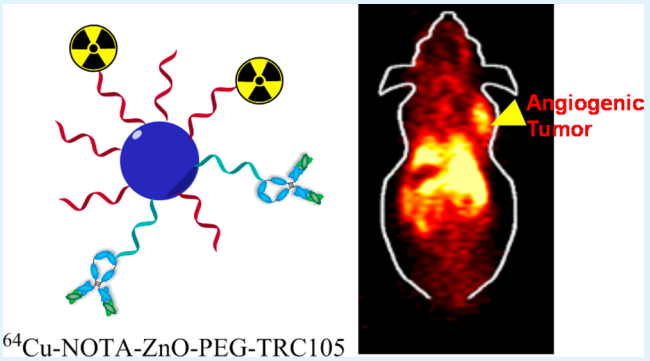

KEYWORDS: *zinc oxide, positron emission tomography, imaging, drug delivery, CD105, angiogenesis*

INTRODUCTION

Significant research efforts have been put into biocompatible nanosized zinc oxide (ZnO) due to its unique physical properties. Nano ZnO has versatile applications in optics, electronics, sensors, drug delivery, and biomedical imaging.[1,2] Particularly, nanosized ZnO possesses high surface areas, excellent interaction with electro-magnetic wave, and tunable electronic properties.[3] Various nanostructures of ZnO have been developed including nanowires, nanotubes, nanopods, and nanorods.[2]

The majority of nano ZnO surface is decorated with hydroxyl groups (−OH), which can be used for further conjugation with various functional molecules.[4] Upon direct contact with aqueous solution, ZnO can dissolve slowly in both acidic (e.g., tumor microenvironment) and strong basic conditions. Since Zn^{2+} is an essential nutrient for adults, ZnO nanomaterials are considered to be safe *in vivo*. In fact, ZnO is graded as a "GRAS" (generally recognized as safe) substance (Code of Federal Regulations Title 21, Section 182.8991) by the U.S. Food and Drug Administration (FDA). With these properties, ZnO nanomaterials can be selected as biocompatible and biodegradable nanoplatforms for targeted cancer therapy.

Molecular imaging can measure the distribution pattern and characterize the interaction events of a given molecule *in vivo*.[5] Among all molecular imaging techniques, fluorescence imaging has intrinsically high sensitivity/safety, optimal spatial resolution, and relatively low instrumentation cost while low tissue penetration is the major curdle for its application.[6] At the same time, positron emission tomography (PET) imaging, which has been widely used for cancer diagnosis and therapy response monitoring, possesses high quantitative capacity and no tissue penetration limitation.[7,8] Since the combination of optical imaging and PET can collect synergistic information on molecular events, our goal here is to produce a ZnO-based nanoparticle (ZnO NP) to serve as a PET and fluorescence image-guided drug delivery vector.[9]

CD105, also known as endoglin, was used as the target on tumor due to its nearly exclusive expression pattern on proliferating endothelial cells (especially inside a tumor).[10,11] In our previous studies, radiolabeled TRC105, a monoclonal

Received: December 2, 2014
Accepted: January 21, 2015
Published: January 21, 2015

DOI: 10.1021/am508440j
ACS Appl. Mater. Interfaces 2015, 7, 3373−3381

Scheme 1. Schematic Synthesis Route of NOTA-ZnO-PEG-TRC105 and NOTA-ZnO-PEG-NH_2

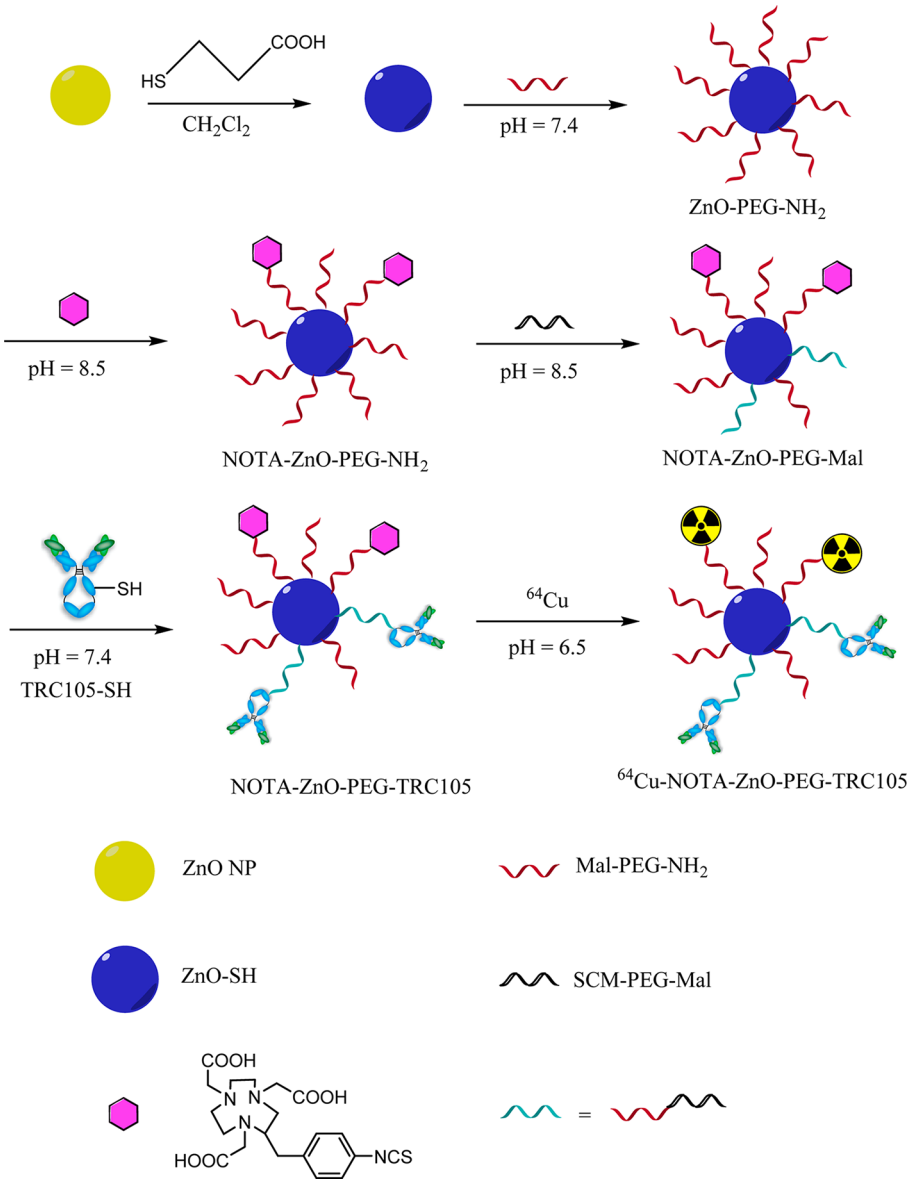

antibody against CD105, was repeatedly used for noninvasive CD105 imaging in various tumor models.[12−17] A recent phase I trial in patients with advanced cancer further confirmed that TRC105 was well tolerated in these patients and could stabilize the disease progression.[18] With the support of current evidence, we can conclude that TRC105 and its derivatives can play important roles in multiple aspects of cancer patient management.

Therefore, we develop a tumor-targeted, PET imageable red fluorescent ZnO NPs in the current study by conjugation with TRC105. Red fluorescent ZnO NPs have been synthesized and used as a potentially theranostic reagent with versatile application potentials. By targeting of CD105 on tumor vasculature, more than a 3-fold higher uptake (~6 %ID/g at 4 h postinjection [p.i.]) in tumor was observed for the TRC105-conjugated ZnO NPs compared to ZnO NPs without TRC105 conjugation (~2 %ID/g at 4 h p.i.). The targeting efficacy, specificity, and biodistribution of these ZnO nanoconjugates were investigated systematically. The TRC105-ZnO NPs designed here can be used as a cancer theranostic nanoplatform in the future upon further optimization.

EXPERIMENTAL SECTION

Synthesis of Red Fluorescent ZnO NPs. Red fluorescent ZnO nanoparticles were synthesized by a calcination method that was reported in the literature.[19] The 0.6 mmol zinc acetate dehydrate, predissolved in 12 mL of dimethylformamide (DMF), was added by droplets to 60 mL of DMF solution containing 0.3 mmol of 2-aminoterephthalic acid and 0.3 mmol of acetylenedicarboxylic acid while stirring. After stirring for 10 min, zinc 2-aminoterephthalate acetylenedicarboxylate coordination polymer formed as yellow precipitates. These precipitates were filtered, washed by DMF, and dried in a vacuum oven at 60 °C for 5 h. The final product was obtained by calcination of the dried powders at 550 °C with an air flow for 75 min after a heating ramp at a rate of 2 degrees per minute. The scanning electron microscopy (SEM) images were taken by LEO 1530 FE-SEM.

Conjugation of ZnO NPs. In this study, the surface of ZnO NPs was functionalized by carboxylic acids that can form bidentate coordination bonds with the zinc atoms. The detailed procedure was previously reported by our group.[20,21] Briefly, 3 mg of 3-

DOI: 10.1021/am508440j
ACS Appl. Mater. Interfaces 2015, 7, 3373−3381

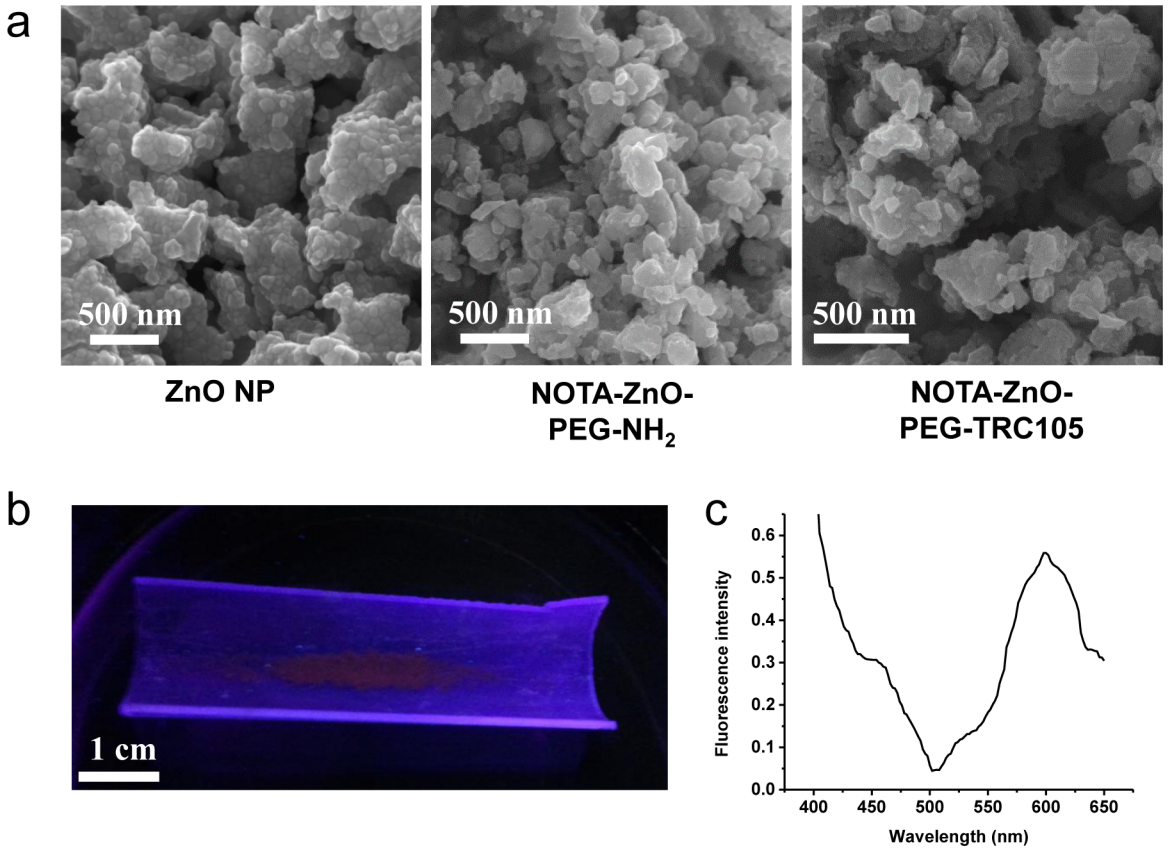

Figure 1. (a) SEM images of ZnO NP, NOTA-ZnO-PEG-NH_2, and NOTA-ZnO-PEG-TRC105. (b) Red fluorescence emitted from ZnO NPs after the excitation from UV light. (c) Fluorescence spectrum of ZnO NPs at the excitation of 350 nm.

mercaptopropionic acid (Sigma-Aldrich, St. Louis, MO) were added into 2 mL of dichloromethane (DCM) suspension of ZnO NPs (3 mg/mL) and stirred at 350 rpm for 1 h (room temperature (RT)). After removing DCM by evaporation, the intermediate product (ZnO-SH) was repeatedly washed by ethanol. In total, 2 mg of ZnO-SH were incubated with 10 mg of maleimide-polyethylene glycol-succinimidyl carboxy methyl ester (Mal-PEG-NH_2; Creative PEGWorks; MW, 5 kDa) for 1 h at RT in 2 mL of phosphate-buffered saline (PBS). Tris(2-carboxyethyl)phosphine hydrochloride (TCEP; Sigma-Aldrich) was also added into the mixture for prevention of thiol oxidation and the final pH was maintained at 7−7.5. The formed ZnO-PEG-NH_2 was purified by 100 kDa cutoff Amicon filter with subsequent wash by ethanol and water. A molar ratio of 1:10 was adopted in the 2 h reaction between ZnO-PEG-NH_2 and S-2-(4-isothiocyanatobenzyl)-1,4,7-triazacyclononane-1,4,7-triacetic acid (p-SCN-Bn-NOTA) at the pH of 8.5. A 100 kDa cutoff Amicon filter was again used to purify the resulting NOTA-ZnO-PEG-NH_2. Another 2 h reaction between NOTA-ZnO-PEG-NH_2 and succinimidyl carboxymethyl PEG maleimide (SCM-PEG-Mal; Creactive PEGWorks; MW, 5 kDa) was carried out at pH 8.5 in a molar ratio of 1:30 to acquire the important intermediate NOTA-ZnO-PEG-Mal.

Meanwhile, the thiolation of TRC105 (named TRC105-SH) was conducted using our previously published procedure.[13] Subsequently, NOTA-ZnO-PEG-Mal was reacted with TRC105-SH (molar ratio 1:5) at pH 7.5 and RT under TCEP protection. The final product, NOTA-ZnO-PEG-TRC105, was purified by centrifugation filtration. The detailed reaction procedures are shown in Scheme 1.

Cellular Uptake Assays. The interactions between ZnO NP conjugates and cellular CD105 were examined by a fluorescence microscope. CD105-positive human umbilical vein endothelia cells (HUVEC[22]) were cultured onto 24-well plates with a density of 1×10^6 per well for overnight. Before treatment with NOTA-ZnO-PEG-TRC105, NOTA-ZnO-PEG-NH_2, or NOTA-ZnO-PEG-TRC105 with TRC105 blocking (0.5 mg/mL TRC105) for 120 min (ZnO concentration, 50 μg/mL), a cell fixing solution (methanol/water/acetic acid, 5:4:1) was used to fix cells. Repeated PBS washing was used after incubation. Fluorescence from ZnO was acquired with a Nikon Eclipse Ti−U inverted microscope (Nikon, Melville, NY) and analyzed using the NIS-Elements BR software.

Animal Model. All animal studies were conducted in compliance with the regulations by the University of Wisconsin Institutional Animal Care and Use Committee. Four- to five-week-old female Balb/c mice from Harlan (Indianapolis, IN) were used for tumor establishment via subcutaneous injection of 2×10^6 cells (formulated in 100 μL of PBS) into the front mouse flank. Caliper measurement (twice per week) was carried out to monitor the tumor sizes. The tumor-bearing animals were used for imaging/biodistribution studies when the tumor diameter reached 6−8 mm.

^{64}Cu-Labeling of ZnO Nanoparticles. In total, 70−120 MBq of $^{64}CuCl_2$ was diluted in 300 μL of 0.1 M sodium acetate buffer (pH 6.5) before incubation with NOTA-ZnO-PEG-TRC105 or NOTA-ZnO-PEG-NH_2 (concentration, ~2 mg/mL) at a ratio of 30 μg per 37 MBq of $^{64}CuCl_2$. The reaction condition is stirring (350 rpm) at 37 °C for 30 min. ^{64}Cu-NOTA-ZnO-TRC105 or ^{64}Cu-NOTA-ZnO-PEG-NH_2 was purified by Amicon filter (molecular weight cutoff, 50 kDa) and resuspended in PBS.

PET Imaging and Biodistribution Studies. PET scans were performed by a Siemens Inveon PET/CT hybrid scanner (Siemens Medical Solutions USA, Inc.) as described previously.[13,22,23] Following the image acquisition, the maximum a posteriori (MAP) algorithm was used for image reconstruction (no attenuation or scatter correction was applied). A tumor-bearing mouse was intravenously injected with 5−10 MBq of ^{64}Cu-NOTA-ZnO-TRC105 or ^{64}Cu-NOTA-ZnO-PEG-NH_2 prior to 3−15 min static PET scans at various time points postinjection (p.i.). The percent injected dose per gram of tissue (% ID/g) of injected materials was also calculated by vendor software (Inveon Research Workplace). Preinjection of TRC105 (1 mg) 1 h before ^{64}Cu-NOTA-ZnO-PEG-TRC105 was also carried out in a

DOI: 10.1021/am508440j
ACS Appl. Mater. Interfaces 2015, 7, 3373−3381

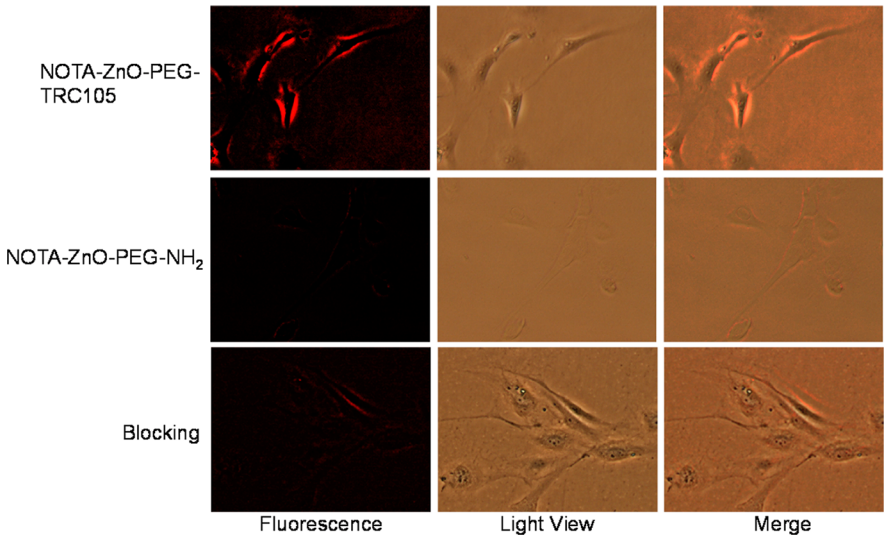

Figure 2. Representative fluorescence images of ZnO NP conjugates in HUVEC (CD105-positive) after 2 h incubation and subsequent washing (images were taken by Nikon Eclipse Ti−U at 200×).

separate group of mice (n = 3) to evaluate the CD105 targeting specificity of ^{64}Cu-NOTA-ZnO-PEG-TRC105. Gamma counter (PerkinElmer) measurements of radioactivity in major tissues/organs (i.e., biodistribution studies) were carried out after the last PET scan in the format of %ID/g (mean ± SD).

RESULTS

Synthesis and Characterization of ZnO Conjugates. A schematic reaction protocol of NOTA-ZnO-PEG-NH_2 and NOTA-ZnO-PEG-TRC105 is shown in Scheme 1. On the basis of SEM measurements, ZnO NP, NOTA-ZnO-PEG-NH_2, and NOTA-ZnO-PEG-TRC105 have the size range of 50−100 nm (Figure 1a). The hydrodynamic sizes of ZnO NP, NOTA-ZnO-PEG-NH_2, and NOTA-ZnO-PEG-TRC105 (measured by dynamic light scattering (DLS)) were 78.4 ± 8.2 nm, 83.3 ± 7.6 nm, and 101.2 ± 10.7 nm, respectively. Although a certain percentage of aggregates (>1 μm) could also be observed in DLS measurement, the overall uniformity of all three samples was high and the samples could stay stable in PBS for over 1 week. Since NOTA is quite small in size, the diameter alteration of the ZnO NP conjugates is primarily from the conjugation of TRC105 (5−10 nm in size) and PEG. The zeta-potential values of ZnO NP, NOTA-ZnO-PEG-NH_2, and NOTA-ZnO-PEG-TRC105 were measured to be −33.2 ± 3.1 mV, −27.3 ± 2.7 mV, and −11.2 ± 2.1 mV, respectively. We notice that NOTA conjugation altered the zeta-potential (i.e., surface charge) of ZnO-NP and so did TRC105 conjugation. TEM and zeta-potential measurements served as strong evidence of NOTA/TRC105 attachment onto ZnO NPs. When excited with UV light (~350 nm), red fluorescence could be observed from ZnO NPs (Figure 1b), which was further confirmed by a fluorescence spectrum measurement to possess a peak emission at 598 nm (Figure 1c).

CD105-Mediated Cellular Uptake. Fluorescent microscopy analysis in HUVEC (CD105 positive[17,22]) and MCF-7 (CD105 negative[17,22]) was used to examine the interaction of NOTA-ZnO-PEG-NH_2 or NOTA-ZnO-PEG-TRC105 with the cells. HUVEC treated with NOTA-ZnO-PEG-TRC105 showed high levels of cellular fluorescence emitted from ZnO NPs. In contrast, cells treated with NOTA-ZnO-PEG-NH_2 showed low levels of cellular fluorescence. Competition of TRC105 (0.5 mg/mL) resulted in significantly decreased cellular fluorescence of NOTA-ZnO-PEG-TRC105 to a level comparable to that of NOTA-ZnO-PEG-NH_2 (Figure 2).

^{64}Cu-Labeling and PET Imaging. ^{64}Cu-labeling, including purification using Amicon filters, took 90 ± 15 min (n = 6). The decay-corrected radiochemical yield was 78.5 ± 10.9% with a radiochemical purity of >95%. Assuming complete recovery of ZnO NPs after Amicon filtration, the ratio of ^{64}Cu activity to ZnO NPs was ~0.97 GBq/mg for both ^{64}Cu-NOTA-ZnO-PEG-NH_2 and ^{64}Cu-NOTA-ZnO-PEG-TRC105.

Despite being CD105-negative in 4T1 cells, 4T1 tumors were used due to their rapid growth speed that leads to abundant tumor angiogenesis and hence expression of high levels of CD105.[12−17] We utilized our previous experience to choose the time points of 0.5, 3, 16, and 24 h p.i. for PET scans following the injection of ^{64}Cu-NOTA-ZnO-PEG-NH_2 or ^{64}Cu-NOTA-ZnO-PEG-TRC105.[13,23−25] The coronal PET slices, containing 4T1 tumors, are presented in Figure 3. The blood pool radioactivity indicated that the few-hour circulation

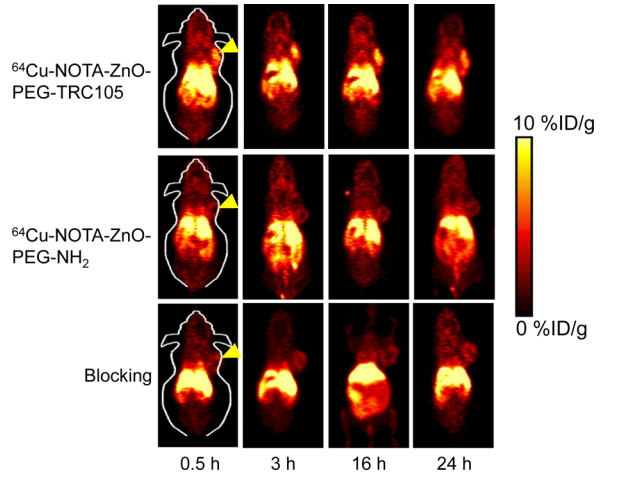

Figure 3. Serial coronal PET images of 4T1 tumor-bearing mice at chosen time points postinjection of ^{64}Cu-NOTA-ZnO-PEG-TRC105, ^{64}Cu-NOTA-ZnO-PEG-NH_2, and blocking group. Yellow arrowheads showed the tumor locations in the mice.

DOI: 10.1021/am508440j
ACS Appl. Mater. Interfaces 2015, 7, 3373−3381

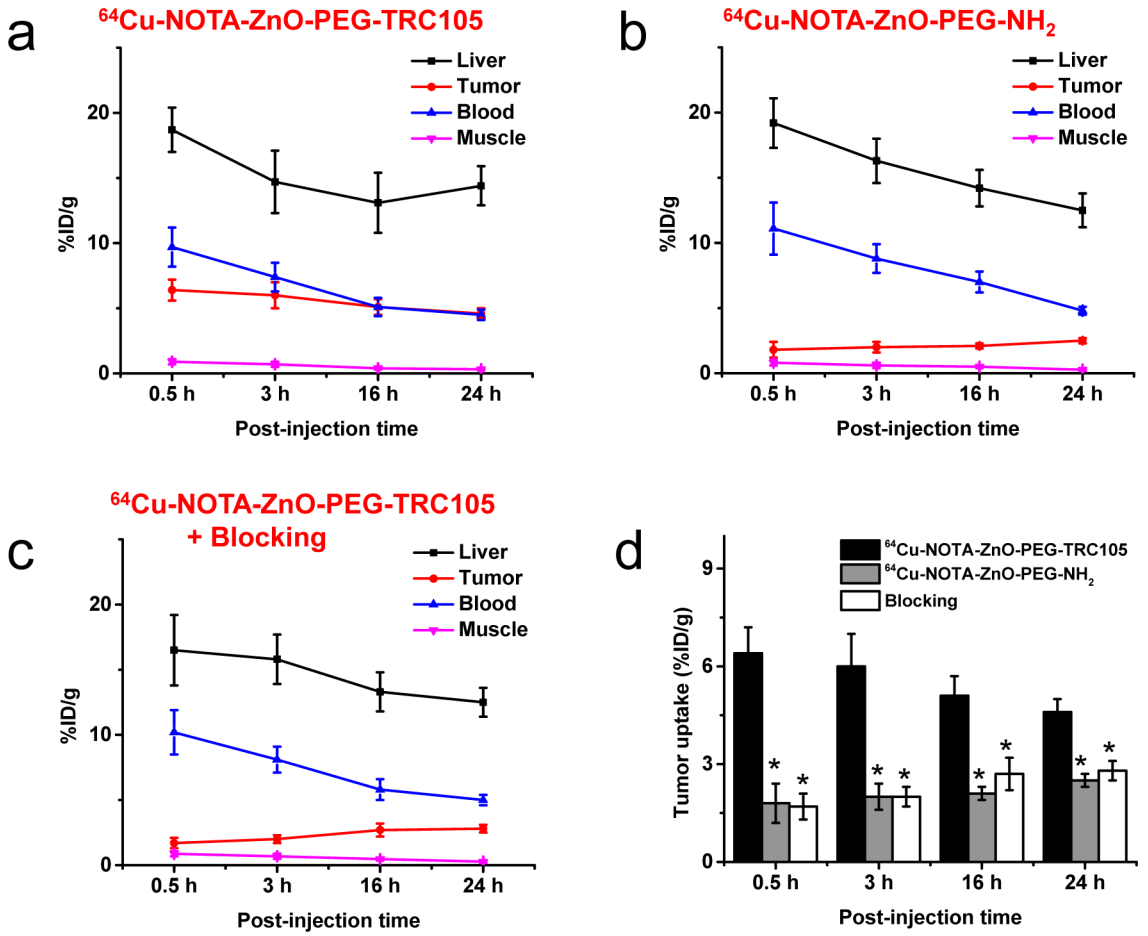

Figure 4. PET region-of-interest (ROI) analysis. Time-activity curves (TAC) of the liver, 4T1 tumor, blood, and muscle were shown p.i. of (a) ^{64}Cu-NOTA-ZnO-PEG-TRC105, (b) ^{64}Cu-NOTA-ZnO-PEG-NH$_2$, and (c) ^{64}Cu-NOTA-ZnO-PEG-TRC105 with a blocking dose of TRC105 (50 mg/kg) are shown (n = 3). The tumor uptakes for these ZnO nanoconjugates were highlighted in part d.

$t_{1/2}$ of ^{64}Cu-NOTA-ZnO-PEG-TRC105 was similar to that of ^{64}Cu-NOTA-ZnO-PEG-NH$_2$. This should be sufficient for *in vivo* tumor targeting. Besides blood, high radioactivity accumulation from ^{64}Cu-NOTA-ZnO-PEG-TRC105 was observable in the liver, tumor, and abdominal area. However, there was no accumulation in most other tissues, thus exhibiting good tumor targeting and image contrast. In comparison, tumor deposit of ^{64}Cu-NOTA-ZnO-PEG-NH$_2$ as well as ^{64}Cu-NOTA-ZnO-PEG-TRC105 with TRC105 blocking (~50 mg/kg) was very low (Figure 3). The detailed quantitative analysis of the PET data will be discussed below.

Quantitative ROI analysis is displayed in Figure 4. The uptake of ^{64}Cu-NOTA-ZnO-PEG-TRC105 in the liver was obvious and demonstrated a gradual decay pattern (18.7 ± 1.7, 14.7 ± 2.4, 13.1 ± 2.3, and 14.4 ± 1.5 %ID/g at 0.5, 3, 16, and 24 h p.i., respectively (n = 3, Figure 4a). The blood retention of ^{64}Cu-NOTA-ZnO-PEG-TRC105 was calculated to be 9.7 ± 1.5, 7.4 ± 1.1, 5.1 ± 0.7, and 4.5 ± 0.4 %ID/g at 0.5, 3, 16, and 24 h p.i., respectively (n = 3, Figure 4a). The penetration of ^{64}Cu-NOTA-ZnO-PEG-TRC105 into 4T1 tumor was fast and stayed stable over the time (6.4 ± 0.8, 6.0 ± 1.0, 5.1 ± 0.6, and 4.6 ± 0.4 %ID/g at 0.5, 3, 16, and 24 h p.i., respectively; n = 3, Figure 4a). Good contrast in the tumor was witnessed by a tumor-to-muscle ratio of 12.1 ± 2.6 for ^{64}Cu-NOTA-ZnO-PEG-TRC105 at as early as 3 h p.i. (n = 3).

^{64}Cu-NOTA-ZnO-PEG-NH$_2$ served as a control to study the accumulation behavior of ZnO NPs without TRC105 conjugation in 4T1 tumors. From Figure 4b, the tumor uptake of ^{64}Cu-NOTA-ZnO-PEG-NH$_2$ (1.8 ± 0.6, 2.0 ± 0.4, 2.1 ± 0.2, and 2.5 ± 0.2 %ID/g at 0.5, 3, 16, and 24 h p.i., respectively; n = 3) was significantly lower than that of ^{64}Cu-NOTA-ZnO-PEG-TRC105 within the whole time frame of PET imaging (p < 0.05; n = 3, Figure 4d). This further confirmed that TRC105 conjugation is the leading factor for the elevated uptake of ^{64}Cu-NOTA-ZnO-PEG-TRC105 in 4T1 tumor. The radioactivity of ^{64}Cu-NOTA-ZnO-PEG-NH$_2$ in the blood was similar to that of ^{64}Cu-NOTA-ZnO-PEG-TRC105 (11.1 ± 2.0, 8.8 ± 1.1, 7.0 ± 0.8, and 4.8 ± 0.3 %ID/g at 0.5, 3, 16, and 24 h p.i., respectively; n = 3).

Administering a high amount of TRC105 (50 mg/kg) reduced the 4T1 tumor uptake of ^{64}Cu-NOTA-ZnO-PEG-TRC105 significantly (1.7 ± 0.4, 2.0 ± 0.3, 2.7 ± 0.5, and 2.8 ± 0.3 %ID/g at 0.5, 3, 16, and 24 h p.i., respectively; p < 0.05, n = 3; Figure 4c,d). This again confirmed the CD105 specificity of ^{64}Cu-NOTA-ZnO-PEG-TRC105 *in vivo*. TRC105 administration did not alter the liver uptake of ^{64}Cu-NOTA-ZnO-PEG-TRC105 (16.5 ± 2.7, 15.8 ± 1.9, 13.3 ± 1.5, and 12.5 ± 1.1 %ID/g at 0.5, 3, 16, and 24 h p.i., respectively; n = 3; Figure 4c).

Biodistribution studies was carried out after the last PET scans (Figure 5a,b). Two more separate groups of mice (n = 4 per group) were injected with ^{64}Cu-NOTA-ZnO-PEG-TRC105

DOI: 10.1021/am508440j
ACS Appl. Mater. Interfaces 2015, 7, 3373−3381

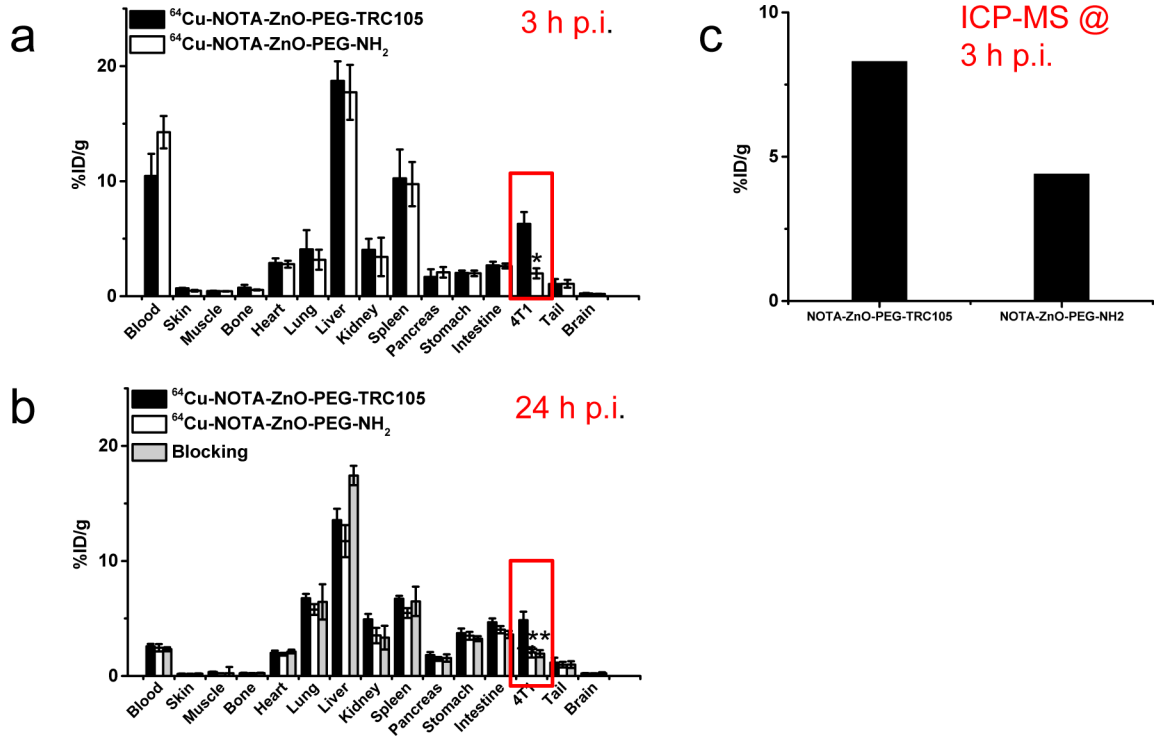

Figure 5. (a) Biodistribution of ^{64}Cu-NOTA-ZnO-PEG-TRC105 and ^{64}Cu-NOTA-ZnO-PEG-NH$_2$, at 3 h postinjection. (b) Biodistribution of ^{64}Cu-NOTA-ZnO-PEG-TRC105, ^{64}Cu-NOTA-ZnO-PEG-NH$_2$, and blocking group (50 mg/kg TRC105 injected 1 h prior to ^{64}Cu-NOTA-ZnO-PEG-TRC105) at 24 h postinjection. (c) ICPMS measurement of tumor homogenates 3 h postinjection of NOTA-ZnO-PEG-TRC105 or NOTA-ZnO-PEG-NH$_2$.

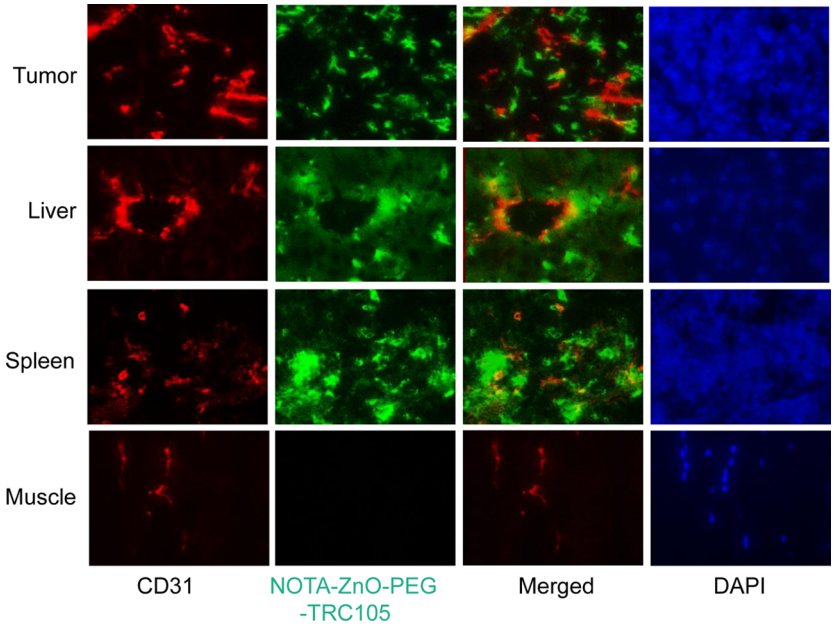

Figure 6. Histological analysis of 4T1 tumor, liver, spleen, and muscle at 3 h postinjection of NOTA-ZnO-PEG-TRC105. Red fluorescence stands for CD31 staining and the location of NOTA-ZnO-PEG-TRC105 is indicated by green fluorescence. Blue fluorescence from DAPI clarified the nuclei locations.

or ^{64}Cu-NOTA-ZnO-PEG-NH$_2$ and used for determination of their distribution profiles at 3 h p.i. (early time point with a peak 4T1 tumor uptake based on PET). Consistent with PET studies, the uptake of ^{64}Cu-NOTA-ZnO-PEG-TRC105 in the 4T1 tumor was higher than all the major organs/tissues except liver and spleen (mostly responsible for clearance). The radioactivity observed in kidneys probably came from two pathways, the degradation of ZnO NPs and/or a small amount of ^{64}Cu detachment from NOTA chelators on the surface of ZnO NPs. In summary, the quantitative data acquired from the biodistribution studies demonstrated good agreement with PET ROI quantification.

At the same time and in order to confirm that the uptake in the tumor is relevant to ZnO NP delivery, we did inductively

DOI: 10.1021/am508440j
ACS Appl. Mater. Interfaces 2015, 7, 3373−3381

coupled plasma mass spectrometry (ICPMS) on excised 4T1 tumors from two individual mice at 3 h p.i. of NOTA-ZnO-PEG-TRC105 or NOTA-ZnO-PEG-NH_2 (5 mg/kg each). Almost 2-fold higher zinc concentration was confirmed in the tumor injected with NOTA-ZnO-PEG-TRC105, when compared to NOTA-ZnO-PEG-NH_2 (8.3 %ID/g and 4.4 %ID/g, respectively (Figure 5c). This matched very well the results from the biodistribution studies and PET scans.

Histology. To confirm that the enhanced ZnO NPs delivery to 4T1 tumor was primarily via the introduction of TRC105, each of three 4T1 tumor-bearing mice was injected with 5 mg/kg of NOTA-ZnO-PEG-TRC105 and euthanized at 3 h p.i. Tissues showing high accumulation of ^{64}Cu-NOTA-ZnO-PEG-TRC105, i.e., the tumor, liver, and spleen, were used for histological analysis. With minimal ^{64}Cu-NOTA-ZnO-PEG-TRC105 absorption, the muscle tissue was used a standard control for normal tissues.

TRC105 attached onto ZnO NPs was used as the primary antibody label, thus only an Alexa Fluor488-labeled antihuman IgG was required for visualization purpose. Based on that, the green fluorescence in Figure 6 was a location indicator of NOTA-ZnO-PEG-TRC105. From the clear separation of the red (stands for CD31, an endothelial cell marker on vessels) and green fluorescence at 3 h p.i., we could confirm significant extravasation of NOTA-ZnO-PEG-TRC105 in the 4T1 tumor at that time. Significant uptake of NOTA-ZnO-PEG-TRC105 in liver and spleen slices at 3 h p.i. (Figure 6) was also observed. We have to emphasize here that the green fluorescence from NOTA-ZnO-PEG-TRC105 displayed a weak overlay with CD31 staining, which indicates that liver/spleen uptake of NOTA-ZnO-PEG-TRC105 was not mediated by CD105. At the same time, green fluorescence was undetectable in muscle.

DISCUSSION

Various nanomaterials have been used in targeted drug delivery to significantly enhance the therapeutic outcome and minimize undesirable side effects. Compared with other nanomaterials, ZnO-based nanomaterials are attractive due to their low toxicity and biodegradable characteristics.[26] On the basis of these desirable properties, ZnO nanomaterials have gained enormous interest in biomedical applications. Different types of chemo/gene drugs (e.g., doxorubicin, daunorubicin, or DNA fragments) have been loaded on ZnO nanomaterials for effective delivery into cancer cells.[2] The data from the current study confirmed the enhanced uptake of ZnO nanoparticles in tumor sites as a result of a targeting ligand (TRC105) conjugation, which could enable ZnO nanomaterials as a tumor-selective drug delivery nanoplatform in the future.

The abundance of −OH groups on the surface of ZnO can be readily functionalized by molecules with various activities.[4,27] Successful surface modification of ZnO-based nanomaterials is critical for both their stability and drug delivery efficacy. Surface PEGylation of ZnO NPs was performed twice in this study to facilitate the attachment of NOTA and TRC105, improve the stability of ZnO NPs in a biological scenario, and reduce the opsonization, thus improving the blood circulation lifetime of ^{64}Cu-NOTA-ZnO-PEG-TRC105. SEM, DLS, and zeta potential characterizations confirmed the successful surface functionalization. Good dispersion in PBS could be achieved for NOTA-ZnO-PEG-TRC105 for weeks.

In vivo distribution profiles of ZnO NPs are very critical for their drug delivery applications. The ZnO NPs showed strong red fluorescence at room temperature (Figure 1b,c). We believe that the fluorescence came from the nonstoichiometric defects, e.g., Zn interstitials or oxygen vacancies associated with the Zn deposition.[28] Such defects usually result in a green fluorescence, sometimes with slightly blue or red shift depending on the synthesis conditions.[29,30] Hence it is very rare and intriguing that the ZnO nanoparticles we synthesized exhibited red fluorescence. In our synthesis, we adopted a polymer condensation method that is largely different from the hydrolysis/alcoholysis used for most other ZnO nanoparticles. In our polymer condensation synthesis, ZnO comes from the condensation of Zn−O−(C═O)− bond in the form of their coordination polymers, while in the prevalent hydrolysis/alcoholysis synthesis, ZnO comes from zinc hydroxide/zinc alcoholoxide. Therefore, the formation mechanism of their intrinsic defects, such as zinc vacancies, oxygen vacancies, as well as their complex defects, may have been radically different. The difference in the species and concentration of such defects may have resulted in a strong defects-related emission at a shifted wavelength. Electron paramagnetic resonance studies suggested that single-ionized oxygen vacancies concentrated on the surface of ZnO nanoparticles may be responsible for the red fluorescence.[19] The fluorescent ZnO NPs coupled with PET imaging capacity can enable the *in vivo* monitoring of ZnO nanomaterials in biomedical applications. Compared with our previously developed green fluorescent ZnO nanowires,[20,21] these red-fluorescing ZnO NPs possess better tissue penetration of the optical signal, making them more preferable for fluorescence-guided drug delivery purposes. However, the requirement of ultraviolet light excitation (excitation wavelength, ∼350 nm) for their fluorescence limited their applications *in vivo*, which serves as the primary reason that no fluorescence imaging was performed *in vivo* in the current study. Further optimization is under way to make red fluorescent ZnO NPs excitable by visible lights. The conjugation of ^{64}Cu onto the surface of ZnO NPs in this study provided an alternative method and enabled the accurate quantification of these ZnO NPs *in vivo* by PET.

CD105 is critical for tumor angiogenesis, with a tremendous potential to serve as a theranostic marker for various tumors based on literature reports.[10,11,31] CD105 exhibits several advantages compared to other markers, which includes the independence from tumor histotype or tumor cell expression, easy circulation accessibility, and universal tumor vasculature expression. The conjugation of TRC105 onto ZnO NPs significantly boosted their interactions with CD105-positive cells (Figure 2) and their tumor vasculature targeting efficacy (Figures 3−5). PET imaging capacity of ^{64}Cu-NOTA-ZnO-PEG-TRC105 makes it more clinically translatable[32−34] and applicable for quantitative and sensitive tumor detection.[35−37]

Different studies have been carried out to assess the cytotoxicity of ZnO nanomaterials and demonstrate that their toxicity is dependent on the sizes, morphologies, surface chemistry, and cell types.[38] Although ZnO-base nanomaterials have been primarily considered to possess no adverse side effects and high biodegradability, the materials' dosage should be kept as low as possible. In the current study, no cell morphology changes were observed by us despite the fact that no toxicity evaluation was carried out. Another potential research direction is to select better ligands on ZnO NPs. Despite all the advantages discussed in the previous text, TRC105 can still interact nonspecifically with Fc receptor from different types of immune cells.[39] To minimize these interactions and the potential immune responses, antibody

DOI: 10.1021/am508440j
ACS Appl. Mater. Interfaces 2015, 7, 3373−3381

fragments or peptides can be used for future generation of the targeted ZnO NP platform.

The versatile surface chemistry of ZnO nanomaterials enables them to be attached with various molecules (e.g., drugs or imaging labels). In this study, radiolabeled ZnO nanomaterials were used for PET imaging and *in vivo* tumor targeting. This biocompatible/biodegradable ZnO nanomaterial platform can be used for future tumor-targeted cargo delivery. Other future research directions of ZnO nanomaterials that are of great importance include the following: (1) combination therapy of cancer (e.g., photo dynamic therapy (PDT) with drug/gene-loaded ZnO nanomaterials); (2) dual-modality imaging (e.g., PET/optical or PET/MRI), which takes advantage of the quantitation capability of PET and the intrinsic fluorescence signal of ZnO (and/or high resolution of MRI) to track ZnO nanomaterials *in vivo*; (3) thorough investigation of the pharmacokinetics and long-term toxicity of ZnO nanomaterials with different surface modifications; among others.

CONCLUSIONS

^{64}Cu-NOTA-ZnO-PEG-TRC105 nanoconjugates were reported in this study for tumor vasculature targeting, imageable by PET. Pharmacokinetics and tumor-targeting efficacy/specificity in 4T1 tumor-bearing mice were thoroughly investigated. Around a 3-fold enhancement of tumor accumulation over passive targeting alone was confirmed due to CD105 targeting. Given the safety and high accommodation of therapeutic agents, as-designed ^{64}Cu-ZnO-PEG-TRC105 could be employed as image-guided drug delivery vectors for theranostic applications. Other targeting ligands could also be conjugated to ZnO NPs for further improvement of tumor accumulation *in vivo*.

AUTHOR INFORMATION

Corresponding Authors

*Fax: 1-608-262-8353. Phone: 1-608-890-2667. E-mail: xudong@engr.wisc.edu.

*Fax: 1-608-265-0614. Phone: 1-608-262-1749. E-mail: wcai@uwhealth.org.

Notes

The authors declare the following competing financial interest(s): Charles Theuer is an employee of TRACON Pharmaceuticals.

ACKNOWLEDGMENTS

We acknowledge the financial support from the University of Wisconsin-Madison, the National Institutes of Health (NIBIB/NCI Grants1R01CA169365 and P30CA014520), the Department of Defense (Grants W81XWH-11-1-0644 and W81XWH-11-1-0648), the Department of Energy (Grant DE-SC0008384), Air Force Office of Scientific Research (Award # FA9550-13-1-0168), and the American Cancer Society (Grant 125246-RSG-13-099-01-CCE).

REFERENCES

(1) Xiong, H. M. ZnO Nanoparticles Applied to Bioimaging and Drug Delivery. *Adv. Mater.* **2013**, *25*, 5329−5335.

(2) Zhang, Y.; Nayak, T. R.; Hong, H.; Cai, W. Biomedical Applications of Zinc Oxide Nanomaterials. *Curr. Mol. Med.* **2013**, *13*, 1633−1645.

(3) Ko, W.; Jung, N.; Lee, M.; Yun, M.; Jeon, S. Electronic Nose Based on Multipatterns of ZnO Nanorods on a Quartz Resonator with Remote Electrodes. *ACS Nano* **2013**, *7*, 6685−6690.

(4) Liu, D.; Wu, W.; Qiu, Y.; Yang, S.; Xiao, S.; Wang, Q. Q.; Ding, L.; Wang, J. Surface Functionalization of ZnO Nanotetrapods with Photoactive and Electroactive Organic Monolayers. *Langmuir* **2008**, *24*, 5052−5059.

(5) Mankoff, D. A. A Definition of Molecular Imaging. *J. Nucl. Med.* **2007**, *48*, 18N−21N.

(6) Moriyama, E. H.; Zheng, G.; Wilson, B. C. Optical Molecular Imaging: from Single Cell to Patient. *Clin. Pharmacol. Ther.* **2008**, *84*, 267−271.

(7) Cai, W.; Chen, X. Multimodality Molecular Imaging of Tumor Angiogenesis. *J. Nucl. Med.* **2008**, *49* (Suppl 2), 113S−128S.

(8) Lopci, E.; Grassi, I.; Chiti, A.; Nanni, C.; Cicoria, G.; Toschi, L.; Fonti, C.; Lodi, F.; Mattioli, S.; Fanti, S. PET Radiopharmaceuticals for Imaging of Tumor Hypoxia: A Review of the Evidence. *Am. J. Nucl. Med. Mol. Imaging* **2014**, *4*, 365−384.

(9) Chakravarty, R.; Hong, H.; Cai, W. Positron Emission Tomography Image-Guided Drug Delivery: Current Status and Future Perspectives. *Mol. Pharm.* **2014**.

(10) Dallas, N. A.; Samuel, S.; Xia, L.; Fan, F.; Gray, M. J.; Lim, S. J.; Ellis, L. M. Endoglin (CD105): a Marker of Tumor Vasculature and Potential Target for Therapy. *Clin. Cancer Res.* **2008**, *14*, 1931−1937.

(11) Seon, B. K.; Haba, A.; Matsuno, F.; Takahashi, N.; Tsujie, M.; She, X.; Harada, N.; Uneda, S.; Tsujie, T.; Toi, H.; Tsai, H.; Haruta, Y. Endoglin-Targeted Cancer Therapy. *Curr. Drug Delivery* **2011**, *8*, 135−143.

(12) Engle, J. W.; Hong, H.; Zhang, Y.; Valdovinos, H. F.; Myklejord, D. V.; Barnhart, T. E.; Theuer, C. P.; Nickles, R. J.; Cai, W. Positron Emission Tomography Imaging of Tumor Angiogenesis with a ^{66}Ga-Labeled Monoclonal Antibody. *Mol. Pharmaceutics* **2012**, *9*, 1441−1448.

(13) Hong, H.; Yang, K.; Zhang, Y.; Engle, J. W.; Feng, L.; Yang, Y.; Nayak, T. R.; Goel, S.; Bean, J.; Theuer, C. P.; Barnhart, T. E.; Liu, Z.; Cai, W. In Vivo Targeting and Imaging of Tumor Vasculature with Radiolabeled, Antibody-Conjugated Nanographene. *ACS Nano* **2012**, *6*, 2361−2370.

(14) Hong, H.; Zhang, Y.; Engle, J. W.; Nayak, T. R.; Theuer, C. P.; Nickles, R. J.; Barnhart, T. E.; Cai, W. In Vivo Targeting and Positron Emission Tomography Imaging of Tumor Vasculature with ^{66}Ga-Labeled Nano-graphene. *Biomaterials* **2012**, *33*, 4147−4156.

(15) Zhang, Y.; Hong, H.; Engle, J. W.; Bean, J.; Yang, Y.; Leigh, B. R.; Barnhart, T. E.; Cai, W. Positron Emission Tomography Imaging of CD105 Expression with a ^{64}Cu-Labeled Monoclonal Antibody: NOTA is Superior to DOTA. *PLoS One* **2011**, *6*, e28005.

(16) Guo, J.; Hong, H.; Chen, G.; Shi, S.; Zheng, Q.; Zhang, Y.; Theuer, C. P.; Barnhart, T. E.; Cai, W.; Gong, S. Image-Guided and Tumor-Targeted Drug Delivery with Radiolabeled Unimolecular Micelles. *Biomaterials* **2013**, *34*, 8323−8332.

(17) Hong, H.; Zhang, Y.; Severin, G. W.; Yang, Y.; Engle, J. W.; Niu, G.; Nickles, R. J.; Chen, X.; Leigh, B. R.; Barnhart, T. E.; Cai, W. Multimodality Imaging of Breast Cancer Experimental Lung Metastasis with Bioluminescence and a Monoclonal Antibody Dual-Labeled with ^{89}Zr and IRDye 800CW. *Mol. Pharmaceutics* **2012**, *9*, 2339−2349.

(18) Rosen, L. S.; Hurwitz, H. I.; Wong, M. K.; Goldman, J.; Mendelson, D. S.; Figg, W. D.; Spencer, S.; Adams, B. J.; Alvarez, D.; Seon, B. K.; Theuer, C. P.; Leigh, B. R.; Gordon, M. S. A Phase I First-in-human Study of TRC105 (Anti-Endoglin Antibody) in Patients with Advanced Cancer. *Clin. Cancer Res.* **2012**, *18*, 4820−4829.

(19) Shi, H. Y.; Deng, B.; Zhong, S. L.; Wang, L.; Xu, A. W. Synthesis of Zinc Oxide Nanoparticles with Strong, Tunable and Stable Visible Light Emission by Solid-State Transformation of Zn(II)-Organic Coordination Polymers. *J. Mater. Chem.* **2011**, *21*, 12309−12315.

(20) Hong, H.; Shi, J.; Yang, Y.; Zhang, Y.; Engle, J. W.; Nickles, R. J.; Wang, X.; Cai, W. Cancer-Targeted Optical Imaging with Fluorescent Zinc Oxide Nanowires. *Nano Lett.* **2011**, *11*, 3744−3750.

DOI: 10.1021/am508440j
ACS Appl. Mater. Interfaces 2015, 7, 3373−3381

(21) Shi, J.; Hong, H.; Ding, Y.; Yang, Y.; Cai, W.; Wang, X. Evolution of Zinc Oxide Nanostructures through Kinetics Control. *J. Mater. Chem.* **2011**, *21*, 9000−9008.
(22) Hong, H.; Yang, Y.; Zhang, Y.; Engle, J. W.; Barnhart, T. E.; Nickles, R. J.; Leigh, B. R.; Cai, W. Positron Emission Tomography Imaging of CD105 Expression During Tumor Angiogenesis. *Eur. J. Nucl. Med. Mol. Imaging* **2011**, *38*, 1335−1343.
(23) Xiao, Y.; Hong, H.; Javadi, A.; Engle, J. W.; Xu, W.; Yang, Y.; Zhang, Y.; Barnhart, T. E.; Cai, W.; Gong, S. Multifunctional Unimolecular Micelles for Cancer-Targeted Drug Delivery and Positron Emission Tomography Imaging. *Biomaterials* **2012**, *33*, 3071−3082.
(24) Shi, S.; Yang, K.; Hong, H.; Valdovinos, H. F.; Nayak, T. R.; Zhang, Y.; Theuer, C. P.; Barnhart, T. E.; Liu, Z.; Cai, W. Tumor Vasculature Targeting and Imaging in Living Mice with Reduced Graphene Oxide. *Biomaterials* **2013**, *34*, 3002−3009.
(25) Yang, X.; Hong, H.; Grailer, J. J.; Rowland, I. J.; Javadi, A.; Hurley, S. A.; Xiao, Y.; Yang, Y.; Zhang, Y.; Nickles, R. J.; Cai, W.; Steeber, D. A.; Gong, S. cRGD-Functionalized, DOX-Conjugated, and ^{64}Cu-Labeled Superparamagnetic Iron Oxide Nanoparticles for Targeted Anticancer Drug Delivery and PET/MR Imaging. *Biomaterials* **2011**, *32*, 4151−4160.
(26) Zhou, J.; Xu, N. S.; Wang, Z. L. Dissolving Behavior and Stability of ZnO Wires in Biofluids: A Study on Biodegradability and Biocompatibility of ZnO Nanostructures. *Adv. Mater.* **2006**, *18*, 2432−2435.
(27) Taratula, O.; Galoppini, E.; Wang, D.; Chu, D.; Zhang, Z.; Chen, H.; Saraf, G.; Lu, Y. Binding Studies of Molecular Linkers to ZnO and MgZnO Nanotip Films. *J. Phys. Chem. B* **2006**, *110*, 6506−6515.
(28) Lin, H. Y.; Cheng, C. L.; Chou, Y. Y.; Huang, L. L.; Chen, Y. F.; Tsen, K. T. Enhancement of Band Gap Emission Stimulated by Defect Loss. *Opt. Express* **2006**, *14*, 2372−2379.
(29) Gong, Y.; Andelman, T.; Neumark, G.; O'Brien, S.; Kuskovsky, I. Origin of Defect-Related Green Emission from ZnO Nanoparticles: Effect of Surface Modification. *Nanoscale Res. Lett.* **2007**, *2*, 297−302.
(30) Tang, X.; Choo, E. S. G.; Li, L.; Ding, J.; Xue, J. Synthesis of ZnO Nanoparticles with Tunable Emission Colors and Their Cell Labeling Applications. *Chem. Mater.* **2010**, *22*, 3383−3388.
(31) Zhang, Y.; Yang, Y.; Hong, H.; Cai, W. Multimodality Molecular Imaging of CD105 (Endoglin) Expression. *Int. J. Clin. Exp. Med.* **2011**, *4*, 32−42.
(32) Gambhir, S. S. Molecular Imaging of Cancer with Positron Emission Tomography. *Nat. Rev. Cancer* **2002**, *2*, 683−693.
(33) Alauddin, M. M. Positron Emission Tomography (PET) Imaging with ^{18}F-Based Radiotracers. *Am. J. Nucl. Med. Mol. Imaging* **2012**, *2*, 55−76.
(34) Grassi, I.; Nanni, C.; Allegri, V.; Morigi, J. J.; Montini, G. C.; Castellucci, P.; Fanti, S. The Clinical Use of PET with ^{11}C-acetate. *Am. J. Nucl. Med. Mol. Imaging* **2012**, *2*, 33−47.
(35) Fakhri, G. E. Ready for Prime Time? Dual Tracer PET and SPECT Imaging. *Am. J. Nucl. Med. Mol. Imaging* **2012**, *2*, 415−417.
(36) Nolting, D. D.; Nickels, M. L.; Guo, N.; Pham, W. Molecular Imaging Probe Development: a Chemistry Perspective. *Am. J. Nucl. Med. Mol. Imaging* **2012**, *2*, 273−306.
(37) van Dongen, G. A.; Ussi, A. E.; de Man, F. H.; Migliaccio, G. EATRIS, a European Initiative to Boost Translational Biomedical Research. *Am. J. Nucl. Med. Mol. Imaging* **2013**, *3*, 166−174.
(38) Roy, R.; Das, M.; Dwivedi, P. D. Toxicological Mode of Action of ZnO Nanoparticles: Impact on Immune Cells. *Mol. Immunol.* **2015**, *63*, 184−192.
(39) Ravetch, J. V.; Bolland, S. IgG Fc Receptors. *Annu. Rev. Immunol.* **2001**, *19*, 275−290.

DOI: 10.1021/am508440j
ACS Appl. Mater. Interfaces 2015, 7, 3373−3381